Folding Dynamics of DNA G-Quadruplexes Probed by Millisecond Temperature Jump Circular Dichroism

K Laouer, M Schmid, F Wien, Pascale Changenet, François Hache

Folding Dynamics of DNA G-Quadruplexes Probed by Millisecond Temperature Jump Circular Dichroism

K. Laouer[1], M. Schmid[1], F. Wien[2], P. Changenet[1] and F. Hache[1]*

1- Laboratoire d'Optique et Biosciences, Ecole Polytechnique, CNRS -INSERM, Institut Polytechnique de Paris, 91128 Palaiseau Cedex, France.

2- Synchrotron SOLEIL, L'orme des merisiers, 91192 Gif sur Yvette, France

KEYWORDS. G-quadruplexes, human telomeres, temperature-jump, time-resolved circular dichroism, folding kinetics.

Corresponding Author

*Pascale Changenet, Laboratoire d'Optique et Biosciences, Ecole Polytechnique, CNRS - INSERM, Institut polytechnique de Paris, 91128 Palaiseau Cedex, France, pascale.changenet-barret@polytechnique.edu

ABSTRACT. G-quadruplexes play important roles in cellular regulatory functions, but despite significant experimental and theoretical efforts, their folding mechanisms remain poorly understood. In this context, we developed a T-jump experiment to access the thermal denaturation and renaturation dynamics of short intramolecular G-quadruplexes *in vitro*, on the time scale of a few hundred milliseconds. With this new set-up, we compared the denaturation and renaturation kinetics of three antiparallel topologies made of the human telomeric sequences d[(5‘-GGG(TTAGGG)$_3$-3’]/Na^+ and d[5’-AGGG(TTAGGG)$_3$-3’]/Na^+ and the thrombin-binding aptamer sequence d[5’-GGTTGGTGTGGTTGG-3’]/K^+, with those of the parallel topology made of the human CEB25 minisatellite d[5’-AAGGGTGGGTGTAAGTGTGGGTGGGT-3’]/Na^+. In all cases, exponential kinetics of the order of several hundred milliseconds were observed. Measurements performed for different initial temperatures revealed distinct denaturation and renaturation dynamics, ruling out a simple two-state mechanism. The parallel topology, in which all guanines adopt an *anti* conformation, displays much slower dynamics than antiparallel topologies associated with very low activation barriers. This behavior can be explained by the constrained conformational space due to the presence of the single-base propeller loops that likely hinders the movement of the coiled DNA strand and reduces the contribution of the entropy during the renaturation process at high temperatures.

Introduction

Besides their three-dimensional structures, the folding dynamics of biomolecules play an important role in their biological functions. While the folding mechanisms of proteins and RNA have been often studied over the past decades, those of DNA have attracted much less attention in comparison, most certainly because the biological relevance of non-canonical DNA structures has only emerged recently. Among them, G-quadruplexes (G4), which result from the hydrophobic stacking of several G-quartets stabilized by metal cations, are known now to be involved in important cellular regulation functions.[1-3] Unlike duplexes, G4s provide a rich set of conformations particularly attractive for the fundamental studies of the folding processes of DNA. Despite recent experimental and theoretical efforts (see [4-6] and references therein), there is not yet a consensual picture of the folding mechanisms of intramolecular G4. Although single molecule techniques have yielded valuable information about the fundamental forces at stake in G4s,[7-9] they have a limited time-resolution preventing the observation of folding/unfolding events faster than a few seconds. On the other hand, many experiments based on rapid mixing methods combined with various spectroscopic detections (absorption, fluorescence of labeled nucleotides, FRET or circular dichroism) allowed the observation of cation-induced G4 folding dynamics, with a time resolution of few milliseconds, starting from unfolded states of DNA.[10-12] The purpose of the present study is to address another aspect of the G4 dynamics, starting from solutions containing folded G4s perturbed from their equilibrium in a reversible manner to investigate the subsequent denaturation and renaturation dynamics. In this regard, we used a unique combination of continuous wave (CW) laser temperature-jump (T-jump) measurements combined with time-resolved UV absorption and circular dichroism detections to assess the G4 conformational changes on a time scale spanning a few ten milliseconds up to seconds after an

abrupt rise or decrease of the temperature. In contrast with single-molecule and stopped-flow approaches coupled with FRET, the CD detection, which is very sensitive to the guanine arrangement in the G4 scaffolds, does not require any specific modifications of DNA.[13]

T-jump combined with UV absorption or FRET detections has long been used for studying the melting dynamics of DNA.[14-17] Recently, pulsed laser T-jump combined with ultrafast time-resolved infrared spectroscopy has been used for studying the melting dynamics of label-free short DNA duplexes on the time scale of a few nanoseconds to the millisecond.[18-20] These structurally sensitive experiments have revealed temporal components of ten to a few hundred nanoseconds and a few microseconds, assigned to the end-fraying and the complete dissociation of the duplexes into single-strands, respectively.[18] Unlike short DNA duplexes, the melting dynamics of short intramolecular G4 are expected to occur on longer time scales,[10, 21] making pulsed laser T-jump initiation inappropriate for probing their dissociation. In this regard, recent developments have been achieved for the use of CW T-jump initiation to access both the denaturation and the renaturation dynamics of biomolecules beyond the millisecond time scale.[22-25] Herein, we present the first study of this type, devoted to G4-forming sequences. We compare the thermal denaturation and renaturation dynamics of four G4-forming sequences: three antiparallel topologies made of the human telomeric sequences Tel21 (d[(5‘-GGG(TTAGGG)$_3$-3’]) and Tel22 (d[5’-AGGG(TTAGGG)$_3$-3’]) and the short thrombin binding aptamer sequence (d[5’-GGTTGGTGTGGTTGG-3’]) and the parallel topology made of the human CEB25 minisatellite sequence 26CEB (d[5’-AAGGGTGGGTGTAAGTGTGGGTGGGT-3’]). This study highlights the different time responses in the return to the thermal equilibrium of all the studied G4s depending whether the DNA is heated or cooled. It also provides evidence of a

distinct dynamical behavior between 26CEB and the antiparallel topologies both in their time response and in their energetic profiles.

Materials and Methods

Samples. Phenol red was purchased from Sigma Aldrich. The G4-forming sequences were purchased from Integrated DNA Technologies with standard desalting. In the following, DNA concentration is expressed in oligonucleotides. All solutions were prepared in ultrapure water delivered by Millipore MilliQ system. Solutions of ca. 0.9 mM of Tel21, Tel22 and 26CEB were prepared in 10 mM sodium phosphate buffer (NaH_2PO_4:Na_2HPO_4, Sigma Aldrich) at pH 7 with 0.135 $molL^{-1}$ or 0.065 $molL^{-1}$ NaCl (Sigma-Aldrich), corresponding to a total Na^+ concentration 150 mM and 80 mM, respectively. Solutions of 0.9 mM of TBA were prepared in 10 mM potassium phosphate buffer (KH_2PO_4:K_2HPO_4, Sigma Aldrich) with 135 mM of KCl (Sigma-Aldrich), corresponding to a total K^+ concentration of 150 mM. It is noteworthy that the pK_a of sodium and potassium phosphate buffers is weakly temperature dependent (ca. 0.025/°C).[26] Before use, the G4 stock solution was heated up to 90°C during 5 min and slowly cooled down at a rate of 1°C/min. The G4 formation and dissociation were checked by heating/cooling experiments by recording the absorption spectra of diluted DNA solutions of ca. 5 μM concentration, at a rate of 1°C/min, on a double-beam CARY100 Biomelt (Agilent) in 1-cm optical path cells. Melting curves recorded by heating and cooling of the G4s were found to be superimposable providing evidence of equilibrium measurements and the absence of higher order G4 structures (dimers) in solutions (see Figure S1).

Synchrotron radiation CD (SRCD) spectra of the studied sequences at a concentration of ca. 0.9 mM in oligonucleotides were recorded at SOLEIL synchrotron (DISCO line) in 30μm or

50 μm optical path CaF_2 cells in sodium or potassium phosphate buffer with NaF or KF to avoid the strong absorption of Cl^- below 200 nm. Typically, the spectra were averaged over 3 scans at the speed of 20 nm/min and measured every 3 or 5°C for increasing temperatures. Melting temperatures T_m determined with SRCD were found to be similar to those determined by UV melting, showing the weak effect of the concentration on the folding processes of these sequences in the range between 0.9 mM and 5 μM.

CW laser T-jump. T-jump was achieved by the direct heating up of water with a 1.5 μm radiation, which is absorbed by the $\nu_2 + \nu_3$ overtone vibration resulting from the combination of the bending and the asymmetric stretching vibration modes of the water molecules. In standard experiments, powerful nanosecond lasers are generally used for the solvent excitation, which yielded a fast temperature rise that starts to decrease after ca. 1 ms due to the heat dissipation.[27-28] To extend the observation time window up to the seconds, CW infrared (IR) excitation sources have been used in combination with single-molecule spectroscopy, microfluidic and very recently with 2D IR spectroscopy.[22, 24-25] In a similar way, we implemented a 5W CW laser diode emitting at 1.5 μm for the sample excitation in our T-jump set-up.[23] The IR beam was focused onto a 150*140 μm^2 spot in a 100 μm optical-path sample cell to ensure the homogeneous heating and cooling of the sample by keeping a weak absorption of the solvent. This requires performing T-jump measurements with a concentration of ca. 0.9 mM in oligonucleotides. The switching of the IR laser was provided by a mechanical shutter with open and closing times of ca. <1ms. Experiments were carried on cycles of a duration of 10 s during which the IR laser was repeatedly switched on after 1 s during 4 s and then switched off for a duration of 5 s.

Measurements of the absorption and the CD changes of the sample were performed by using of the third-harmonic of a quasi-CW tunable Titanium-Sapphire oscillator (Millenia+Tsunami

Spectra-Physics) in a two-stage BBO frequency converter as the probe. Depending on the sample, the probe wavelength was tuned to 293 or 266 nm and focused onto a 50 μM diameter spot in the sample cell. The probe circular polarization was modulated at 50 kHz with a photoelastic modulator (Hinds Instruments) before to be sent onto the sample. The transmitted beam was then collected with a rapid photomultiplier tube and demodulated by a lock-in amplifier (Standford Research Systems SR830). With this set-up, the CD and the absorption changes of the samples could be measured simultaneously with a 500 MHz oscilloscope (Tektronix TDS 3052B). All the time-resolved measurements were achieved with a time resolution of 1 ms corresponding to the minimum integration time on the lock-in amplifier necessary for obtaining measurable CD signals. Measurements were averaged over 256 acquisitions to reach a precision of ca. 10^{-5} for the CD measurements. Measurements were performed for different initial temperatures (T_{ini}) corresponding to the sample temperature before the IR irradiation, *i.e.* between 0 and 1 s. In the following, the differential absorbance, $\Delta A(t)$, is the difference in the sample absorbance measured before and after the T-jump:

$$\Delta A(t) = A(t) - A_0 \quad (1)$$

with A(t) the sample absorbance after the T-jump and A_0 the sample absorbance measured before the T-jump. The measured CD signals are the difference in the absorbance of the left- and the right-circularly polarized probe:

$$CD(t) = A_L(t) - A_R(t) \quad (2)$$

with A_L and A_R the sample absorbance for the left and the right circular polarization of the probe, respectively. The ΔA and the CD changes as function of the time are given in optical density (OD).

Heating and cooling time scales of aqueous solutions. Measurements of heating and cooling rates of aqueous solutions *in situ* were achieved with a precision of ± 1°C, by using the phenol red pH indicator in 100 mM tris buffer (pH 7.4), as described in Supporting Information. In order to obtain rapid heating and cooling rates, 1 mm thick CaF_2 cell windows were used, the thermal conductivity of which being ca. 7 times greater than those of silica. In those conditions, heating and cooling were found to be biphasic processes, as illustrated in Figure 1. Sample heating, for a T-jump of 10°C, exhibits a biexponential rise with a dominant fast component of 14 ± 1.3 ms (83%) and slow one of 1.3 s (17%). Sample cooling is slightly slower and displays a biexponential decay with the time constants of 30 ± 2.2 ms (82%) and 1.7 s (18%), respectively. Such multiphasic change of the temperature has been already observed under similar experimental conditions and discussed in details in reference 22. Importantly, as previously reported, both heating and cooling dynamics are found to be independent of the initial temperature and the T-jump amplitude (for details see Supporting Information).

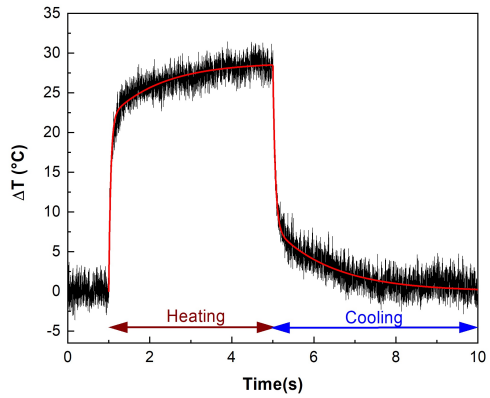

Figure 1: Heating and cooling dynamics measured at 293 nm with the phenol red in 100 mM tris buffer (pH 7.4), after a T-jump of 29 °C after 1s. Red lines correspond to the biexponential fits of the heating and cooling phases indicated by the brown and blue arrows, respectively.

Data analysis. The major issue in these experiments was to extract the intrinsic denaturation and renaturation times of G4 from the experimental data. In this regard, the biphasic heating and cooling of the sample, which may distort the measured kinetics of DNA, has to be taken into account in the fitting procedure. This procedure is described in details in Supporting Information. The basic principle consists in introducing the time dependence of the T-jump in the differential equations of the variation of the unfolded population between the initial and the final temperature of the sample. Knowing from the phenol red measurements, the precise dynamics of the temperature change *in situ*, it is possible to simulate, from the equilibrium UV and CD melting curves, the evolution of the DNA absorption and CD changes expected if the thermal denaturation and renaturation of DNA were faster than the sample temperature change and followed the dynamics of the temperature change of the solvent. As seen in the following, we clearly observe slower denaturation and renaturation kinetics for all the studied G4-forming sequences. Their analysis with a unique relaxation time allowed satisfactory adjustments with an error of ca. 20%. Note that this simple fitting model is used to quantify and discuss the observed denaturation and renaturation times and is not intended to provide the precise kinetic model of G4 folding and unfolding mechanisms. Since T-jump experiments measure the return to the thermal equilibrium after a perturbation of the sample temperature, those times correspond to a combination of the G4 unfolding and folding rate constants. The determination of these elementary rates is however not possible without introducing a precise kinetic model of the mechanisms underlying the thermal denaturation and renaturation processes of DNA.

Results

Antiparallel topologies. The present investigations focused on the two short human telomeric sequences, Tel21 and Tel22 in the presence of 150 mM Na^+ and the 15-mer thrombin binding aptamer sequence, TBA, in the presence of 150 mM K^+. Under these conditions, these sequences are known to assume antiparallel topologies.[29-30] Tel21 and Tel22 are simple models of human telomeric G4s whose potential applications are of primary importance in anti-cancerous strategies.[31] On the other hand, TBA is an artificial DNA sequence known to inhibit blood coagulation due to its ability to specifically bind to thrombin.[32-33] Importantly, TBA is among the shortest intramolecular G4s that therefore is of particular interest for theoretical simulations, notably for disentangling G4 folding processes.[34-39]

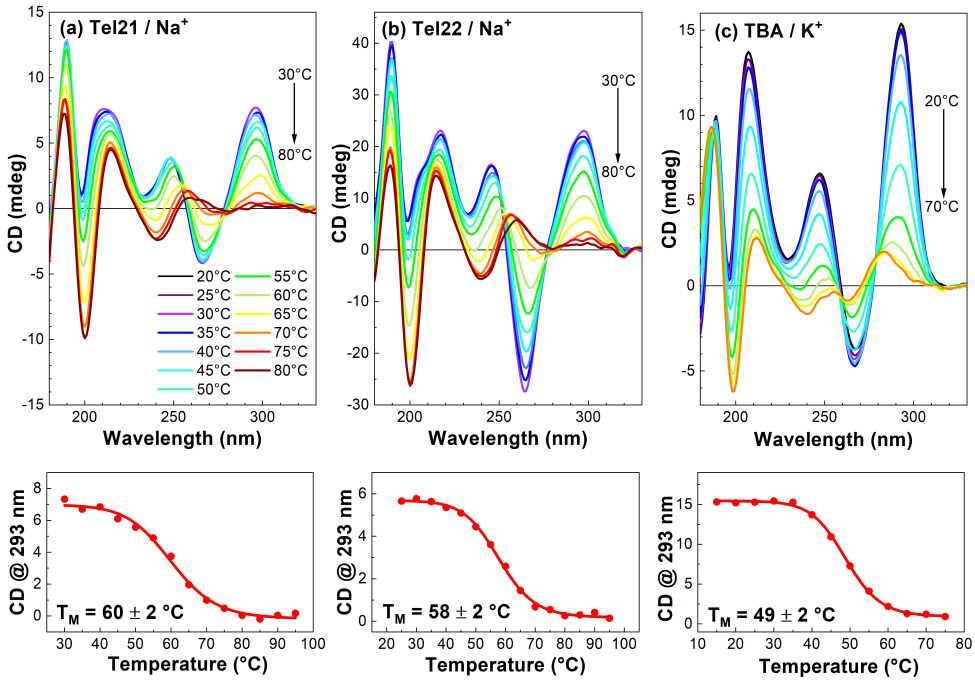

Figure 2: Synchrotron radiation CD (SRCD) spectra and extracted melting curves at 293 nm for (a) Tel21, (b) Tel22 with 150 mM Na^+ and (c) TBA with 150 mM K^+, measured for increasing temperatures with a step of 5°C.

Figure 2 illustrates the steady-state SRCD spectra of ca. 0.9 mM of Tel21/Na^+, Tel22/Na^+ and TBA/K^+ measured at SOLEIL synchrotron, for various temperatures. Despite the presence of several conformations,[29] the CD spectrum of Tel21/Na^+ at room temperature display similar features to that of Tel22/Na^+ known to adopt one basket-type antiparallel conformation made of three guanine tetrads connected by 3 TTA loops, showing that antiparallel topology prevails. In the presence of K^+, TBA is known to form a stable chair-like antiparallel conformation made of two tetrads connected by two lateral TT loops and one lateral TGT loop.[40] Like Tel21/Na^+ and Tel22/Na^+, the SRCD spectra of TBA/K^+ display the characteristic spectral signatures of the antiparallel topologies of G4s with a negative peak and a positive peak centered around 265 nm and 295 nm, respectively.[13, 41] Those signals are representative of the guanine arrangement in the G4 core, arising from the excitonic coupling of the two low-lying electronic π-π* transitions of the purines.

As shown in Figure 2, the fits of the SRCD melting curves at 293 nm assuming a two-state equilibrium (folded ↔ unfolded) yield melting temperatures (T_m) of 60 ± 2 °C for Tel21/Na^+, 58 ± 2 °C for Tel22/Na^+ and 49 ± 2°C for TBA/K^+. Similar values were obtained by UV melting for diluted solutions of ca. 5 μM (see Table S1). In order to investigate the effect of the cation concentration on the G4 denaturation and renaturation dynamics, Tel21 was studied in the presence of 80 mM Na^+. We observed a decrease of ca. 3°C in T_m with respect to Tel21 with 150 mM Na^+, denoting the destabilization of the G4 scaffold. All of these thermodynamic parameters are comparable to those found in previous studies under similar conditions.[11, 42-45]

Taking advantage of the spectral signatures of antiparallel G4s, we measured the denaturation and the renaturation dynamics of Tel21/Na^+, Tel22/Na^+ and TBA/K^+ by T-jump experiments combined with time-resolved absorption and CD detections at 293 nm. Figure 3 displays typical

ΔA and CD changes measured for Tel21 with 80 mM Na^+. After 1 s, when the IR-heating laser diode is switched on, the amplitude of the ΔA and the CD signals drops down within a few 100 ms due to the G4 denaturation. After 5 s, when the IR-heating irradiation is stopped, a slow increase of the ΔA and the CD signals is observed, resulting from the G4 renaturation back to the initial state. As shown in Figure S4, the temporal evolution of the ΔA and the CD signals is found to be similar, providing evidence that, on this time-scale, these measured signals mainly reflect the cooperative change of the secondary structure of DNA. The heat-induced decrease in the G4 absorption is due to the hypochromism at 293 nm characteristic of the unfolding of G4 scaffold (see Figure S1).[42, 46] As can be seen in Figure 3, at this wavelength, the relative variation of the CD resulting from a temperature rise of 20°C is also very strong. It is consistent with that observed in the equilibrium CD melting curves, indicating the complete return to equilibrium of DNA during the probed time scale. As shown in Figure 3, we indeed observe the return of the ΔA and CD signals to their initial values after the cooling phase, providing further evidence that the renaturation is complete after 9 s. In addition, preliminary conventional T-jump measurements performed on telomeric sequences did not reveal any observable change at 293 nm on the time window of a few nanoseconds to the millisecond, indicating that no cooperative dynamical changes occur in the G4 scaffold, at this shorter time scale.[47] This is in contrast to the very first T-jump measurements performed on Tel22/Na^+ with a conventional setup combined with a absorbance detection at 260 nm which is not specifically characteristic of the G4 scaffolds that led the observation of noticeable changes in the absorbance of DNA for a final temperature of 25°C.[48] Those changes that are observed at a temperature much lower than the melting temperature of Tel22 most likely result from non-cooperative changes in DNA rather than the unfolding of the G4 scaffold.

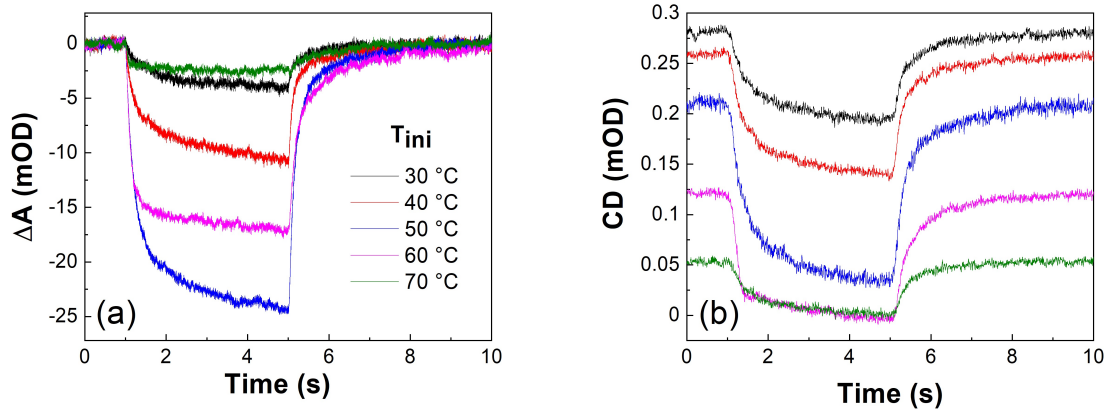

Figure 3: (a) ΔA and (b) CD changes measured at 293 nm for Tel21 with 80 mM Na^+, following a T-jump of 20°C after 1 s and a subsequent cooling down to the initial temperature after 5 s, for various T_{ini} indicated in panel (a).

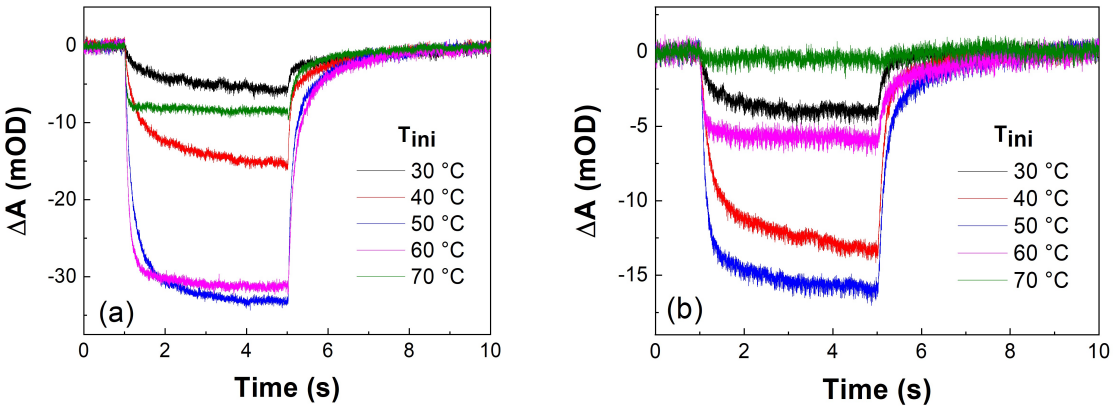

Figure 4: ΔA measured at 293 nm, for (a) Tel22 with 150 mM Na^+ and (b) TBA with 150 mM K^+, following a T-jump of 10°C after 1 s and a subsequent cooling down to the initial temperature after 5 s, for various T_{ini}.

Figure 4, displays ΔA measured for Tel22 with 150 mM Na^+ and TBA with 150 mM K^+. They display a similar behavior to that of Tel21. The denaturation and the renaturation times were extracted from the analytical fitting of the experimental data, as described in the

experimental part. Figure 5 illustrates such analysis for Tel21 with 150 mM Na^+. The blue lines correspond the simulation of the solvent temperature change. As a matter of fact, the measured kinetics presents a time lag corresponding to the intrinsic G4 dynamics. The red lines illustrate their fits with a kinetic model of two interconverting species taking into account the biexponential rates of heating and cooling of the solvent. It is now well established that the folding mechanism of G4 is much more complex than a two-state model, implying population of intermediate states or conformational traps attributed to "extreme kinetic partitioning mechanisms".[49] In the present case, thermal denaturation and renaturation of G4s can be reasonably fitted with an exponential function. It is worth noting that biexponential fits did not yield reliable results about the presence of an additional time component.

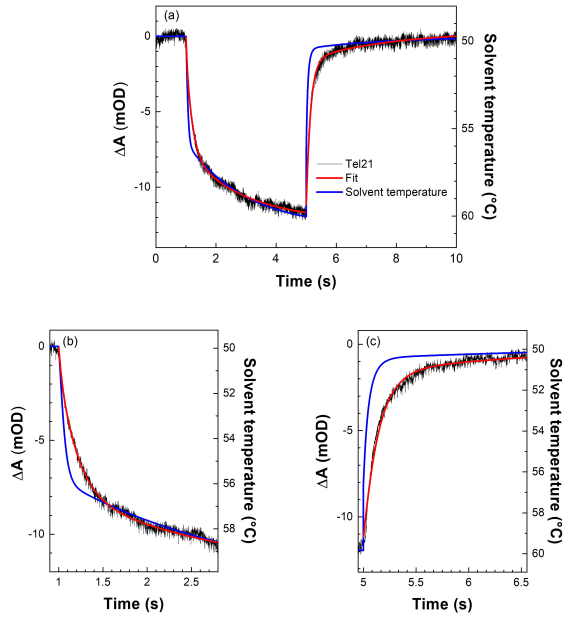

Figure 5: (a) ΔA (black lines) measured at 293 nm, for Tel21 with 150 mM Na^+, following a T-jump of 10°C after 1 s, for T_{ini} = 50 °C, and a subsequent cooling down to the initial temperature after 5 s, (b) ΔA observed during 1.5 s after the T-jump and (c) after the cooling down. Blue lines correspond to the simulation of the solvent temperature change. Red lines correspond to the fits

of the experimental data with a model of two interconverting species "convoluted" with the solvent temperature change.

Time components extracted from the analytical fittings of the experimental data associated the three studied antiparallel topologies for various T_{ini} are gathered in Table 1. They are of the order of a few hundred milliseconds, except for T_{ini} above 70°C for the human telomeric sequences and 60°C for TBA, for which the denaturation times are significantly shorter and the unfolded population exceeds 90%. Interestingly, for each T_{ini}, distinct denaturation and renaturation rates are observed. This excludes a simple two-state folding mechanism for which similar denaturation and renaturation rates equal sum of G4 folding and unfolding rates are expected.

T_{ini}(°C)	Tel21 80mM Na^+		Tel21 150 mM Na^+		Tel22 150 mM Na^+		TBA 150 mM Na^+	
	τ_{Denat} (ms)	τ_{Renat} (ms)	τ_{Denat} (ms)	τ_{Renat} (ms)	$\tau_{Denat.}$ (ms)	τ_{Renat} (ms)	τ_{Denat} (ms)	τ_{Renat} (ms)
30	267	419	*n.m.*	*n.m.*	820	1749	128	148
40	204	192	308	897	351	588	125	107
50	167	140	165	170	163	209	75	138
60	80	239	118	192	73	221	38	318
70	10	641	54	297	30	306	*n.m.*	*n.m.*

Table 1: Thermal denaturation and renaturation times, extracted from the fits of ΔA at 293nm, measured for antiparallel G4 topologies, after a T-jump and a cooling down of 10°C, for different T_{ini} (*n.m.*: not measurable).

Minisatellite G4 sequence 26CEB. For the study of the parallel G4 topology, we chose the well-characterized 26CEB sequence corresponding to a part of the human minisatellite locus motif, CEB25. In the presence of K^+, this 26-mer sequence is known to form a parallel-stranded G-quadruplex involving a 9-nt central double-chain-reversal loop and two other one-base propeller loops.[50-51] The G4 scaffold is further stabilized by the formation of a Watson-Crick

base pair between A2 and T18 anchoring the central loop to the top the 5' G-tetrad.[50] A parallel topology has been also inferred in the presence of Na^+ from CD spectroscopy.[52] The use of Na^+ instead K^+ induces a destabilization of the G4 structure making T-jump measurements more amenable. The measured SRCD spectra for increasing temperatures illustrated on Figure 6 is indeed found to be similar to that of 26CEB with K^+. They display a positive peak at 260 nm and a negative one at 240 nm characteristic of the parallel G4 topology. The SRCD changes at 260 nm yield T_m=56 ± 2 °C.

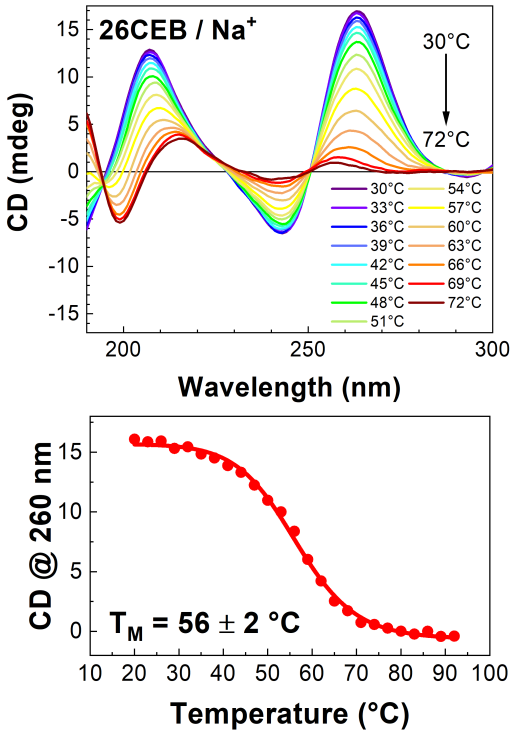

Figure 6: SRCD spectra of 26CEB, with 150 mM Na^+ measured for increasing temperatures with a step of 3°C.

In order to capture the thermal-induced changes in the CD of 26CEB, T-jump experiments were performed at 266 nm. Note that parallel and antiparallel G4 topologies exhibit CD signals

of opposite sign in this spectral region, giving the opportunity to probe the formation of possible intermediates in the two topologies. Figure 7 shows typical CD signals measured for 26CEB with 150 mM Na^+, for different initial temperatures, after a T-jump and a subsequent cooling down of 20°C. It is worth noting the lower signal to noise ratio of these measurements in comparison with the previous one carried at 293 nm. This effect is due to the higher absorbance of DNA at 266 nm with respect to 293 nm that drastically decreases the probe intensity. The measured absorption changes of 26CEB, upon T-jump at 266 nm are given in Figure S5. They display a prominent instantaneous rise and decay at the delay of 1s and 5s, respectively, arising from the contribution of non-cooperative events that clearly appear in the equilibrium UV melting curve of 26CEB at 265 nm as the very strong baselines (see Figure S2) and interfere with the absorption measurements at this particular wavelength.[53] These events may have different origins such as, for instance, the loss of the base stacking or the change of the heat capacity, as the temperature increases. As seen in Figure 7, these contributions are much smaller in the CD signals of CEB26 at 266 nm that we chose to analyze and discuss in the remainder.

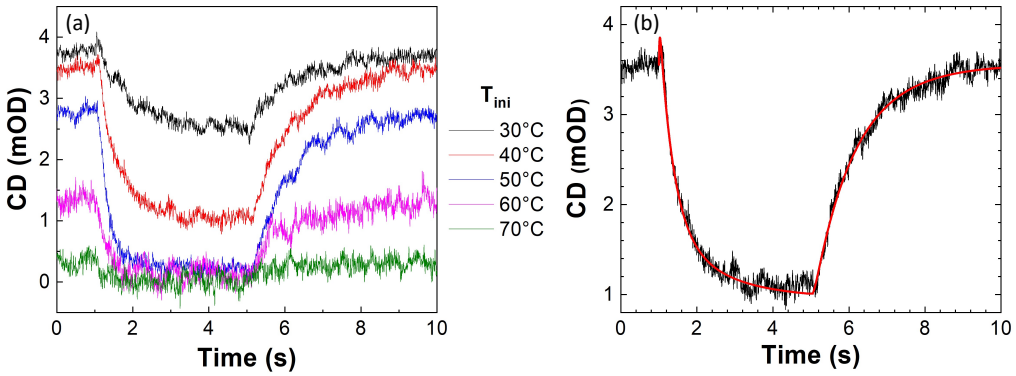

Figure 7: (a) CD changes at 266 nm, measured for 26CEB with 150 mM Na^+, following a T-jump of 20°C after 1 s and a subsequent cooling down to the initial temperature after 5 s, measured for 5 different T_{ini} (b) CD changes measured for T_{ini} = 40°C. Red lines correspond to

the fits of the experimental data with a model of two interconverting species "convoluted" with the dynamics of the solvent temperature change.

As expected from the equilibrium SRCD melting (Figure 6), the CD changes exhibit a slow decrease after the T-jump at 1 s, followed by a slow increase back to its initial value after 5s, during the cooling period. Table 2 gathers the denaturation and renaturation time constants extracted from the exponential fits of the CD changes measured for 26CEB for different T_{ini}. The fits of the ΔA signals in the time range of a few hundred milliseconds yielded comparable values providing evidence that the same cooperative processes are probed in both cases, on this time scale. Like for antiparallel topologies, distinct denaturation and renaturation times are observed for each T_{ini}.

T_{ini}(°C)	τ_{Denat} (ms)	τ_{Renat} (ms)
20	715	1041
30	554	1085
40	357	936
50	237	844
60	227	811
70	120	646

Table 2: Thermal denaturation and renaturation times, extracted from the exponential fits of the CD changes at 266 nm, measured for 26CEB (150 mM Na^+), after a T-jump and a cooling down of 10°C, for different T_{ini}.

Discussion

We performed a comparative study of the thermally-induced denaturation and renaturation dynamics for three G4 antiparallel topologies with one parallel topology. All measured kinetics

were satisfactorily fitted with an exponential function yielding time components ranging from tens of milliseconds to one second. This behavior differs from the multiphasic cation-induced folding processes observed by rapid-mixing methods.[10-12, 21, 54-55] Note that most of these studies have been performed on human telomeric sequences in K^+ solutions, known to form an equilibrium between two hybrid structures which complicates interpretations.[10, 12] Single-molecule FRET approaches also highlighted deviation from a two-state behavior in the folding of several human telomeric sequences.[56-62] However different behaviors have been reported for identical sequences,[56, 60] pointing the importance of the experimental conditions under which such experiments are conducted.[61] Beyond human telomeric G4 polymorphism, multiphasic processes have been recently reported for a parallel topology derived from the c-MYC promoter by fast-mixing methods and attributed to the formation of several intermediates in its cation-induced folding mechanism.[21, 55] Both ensemble and single molecule approaches have led to a large variety of folding and unfolding rates for short intramolecular G4 structures spanning milliseconds to hours, providing evidence of their very complex energy landscapes.[49, 63] In this context, recent theoretical studies gave support to the idea of "extreme" kinetic partitioning folding mechanisms characterized by the existence of multiple competing basins in their folding landscapes.[49, 64] The basic feature of such mechanism is the dependence of the folding pathways on the external conditions, such as the initial folding conditions or the nature of the applied perturbation. This has been clearly shown in the case of the unfolding processes of RNA hairpins by using single-molecule force spectroscopy.[65-67] In stark contrast to stop-flow methods that probe cation-induced folding kinetics from a fully denatured ensemble in absence of cations, T-jump experiments explore the folding dynamics from a thermal equilibrium of folded and unfolded states of DNA in the presence of cations. We therefore think that the observed

differences in the kinetic behavior of G4s stems from the distinct population of unfolded states that is reached with these two different methods, as previously reported for the study of the folding of small DNA hairpins by a combination of T-jumping and rapid mixing experiments.[17]

In order to get additional information on the driving force controlling the folding processes of G4s, Figure 8 displays the variation of the denaturation and renaturation rates extracted from the fitting of our raw experimental data (Tables 1 and 2), as function of the temperature. It is worth recalling that those rates correspond to the return to equilibrium after a sudden increase or decrease of the sample temperature and therefore reflect the contributions of the elementary rates of G4 folding and unfolding. Figure 8 illustrates the distinct dynamic behavior of the aforementioned G4 denaturation and renaturation processes, ruling out the scenario of a simple two-state model suggested at first glance by their exponential kinetics. Whereas the denaturation process of all studied G4s displays an Arrhenius-like behavior, the renaturation rates exhibit a bell-shaped curve with a maximum rate close to T_m, except for the parallel 26CEB which shows an Arrhenius-like behavior.

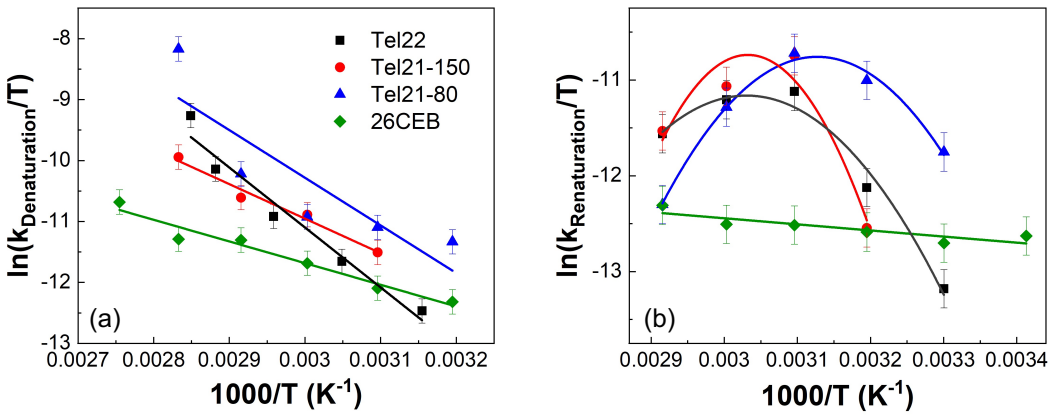

Figure 8: Variation as function of the temperature of (a) the denaturation and (b) the renaturation rates of Tel21, Tel22 and TBA extracted from time-resolved absorption measurements and

26CEB extracted from time-resolved CD measurements. Solid lines illustrate the linear and the parabolic fits of the experimental data.

Table 3 gathers the activation enthalpies extracted from the linear fits of Figure 8 for G4 thermal denaturation. The fits yield activation enthalpies varying between 7 and 19.6 kcal/mol. It is noteworthy that the TBA denaturation exhibits a significantly lower activation enthalpy than the human telomeric sequences, which can be explained by its reduced number of G-tetrads.

Sequence	**Topology**	$\Delta H^{\#}_{Denat}$ **kcal.mol^{-1}**
Tel22-150mM Na^+	Antiparallel	19.6 ± 2.3
Tel21-150mM Na^+	Antiparallel	11.3 ± 1.1
Tel21-80mM Na^+	Antiparallel	15.5 ± 6.8
TBA-150mM K^+	Antiparallel	8.1 ± 2.4
26CEB-150mM Na^+	Parallel	7.1 ± 0.7

Table 3. Activation enthalpies for the thermal denaturation process of the studied G4-forming sequences extracted from the linear fits of Figure 8.

It is clear from this analysis that G4 denaturation rates, which are within a few tens to hundreds milliseconds, cannot be sought in their activation energies that are actually very moderate but instead in the roughness of their folding landscapes. Similar conclusions were drawn for DNA hairpins for which intra-strand interactions, notably stacking interactions in the loops, were introduced as an efficient roughness of their folding landscapes.[68] As a matter of fact, significantly larger heat capacity changes attributed to the strong competition of intra-strand stacking with the folding of guanine-rich sequences have been reported for G4s with respect to DNA duplexes.[43]

In stark contrast with denaturation, the renaturation rates of the antiparallel topologies are found to exhibit a bell-shaped behavior with the temperature. Note that a bell-shaped behavior

has already been reported for cation-induced folding rates of Tel21 with K^+.[12] In fact, such a behavior is reminiscent to proteins and oligonucleotides.[69-71] As shown in Figure 8, at temperatures below T_m the renaturation rates display an Arrhenius-like behavior indicating that the renaturation of the antiparallel topologies is dominated by enthalpy. Then, as the temperature increases, the renaturation rates reach a maximum close to T_m and then decrease. In other words, at temperatures above T_m, the configurational space that has to be explored to refold gets much broader and the reaction becomes entropy-limited.[69]

The most striking difference between the studied antiparallel topologies and the parallel 26CEB is that both the denaturation and renaturation processes of 26CEB exhibit an Arrhenius-like behavior. In addition, the denaturation and renaturation rates of 26CEB are markedly slower than those of Tel21 and Tel22 made of DNA strands of similar length. All the studies carried out to date agree on the fact that the folding rates of parallel topologies are significantly slower than those of anti-parallel topologies.[21, 55, 72-73] It comes out from the present study that the slow denaturation and renaturation rates of 26CEB are associated to very low activation enthalpies of 7 kcal/mol and 1.3 kcal/mol, respectively. Therefore, the slower thermal denaturation of 26CEB compared to that of Tel21 and Tel22 is clearly not due to an increase in activation energy. It could be sought in the presence of the long 9nt central loop, since it has been shown very recently that parallel topologies with a long unstructured central loop exhibit slower folding kinetics than those with a short central loop.[55] However, an increase in the contribution of entropy in the renaturation process could be expected in this case. But we observe instead a decrease in the effect of the entropy in the renaturation process of 26CEB at high temperatures with respect to that of the telomeric sequences. Therefore, we think that the main difference with Tel21 and Tel22 may stem from the presence of the 2 short propeller loops in the parallel

structure conferring a special rigidity to the quadruplex scaffold. This feature could, on one hand, hamper the motion of the bases and thus slow down the folding/refolding processes and, on the other hand, strongly limit the configurational space accessible to the unfolded strands, attenuating the entropic dependence of the renaturation process at high temperatures.

Conclusion

Herein, we performed a comparative study of the dynamical properties of three antiparallel G4s made of the human telomeric sequences, Tel21 and Tel22 and the thrombin-binding aptamer sequence, TBA, with that of the parallel G4 formed from the 26-mer G-rich fragment of the CEB25 motif. In contrast with the previous works on G4s, kinetics measurements were carried out in the vicinity of the thermal equilibrium, by using a CW optical heating method combined to time-resolved detection by UV-visible absorption and CD spectroscopy. Such a method allowed us to investigate for the first time the dynamics of the thermal denaturation and renaturation of the G4s on the time scale of a few ten milliseconds to seconds. All the measured kinetics were satisfactorily fitted with an exponential function associated to a time constant varying between a few ten to a few hundred milliseconds which is more than three order of magnitude slower than hairpins of similar length.[74-75] Despite this "apparent" two state behavior, their dependence with the temperature reveals complex folding mechanisms that can be explained by the large internal friction of the guanine-rich sequences due to their extremely rugged energetic landscapes. The renaturation of the antiparallel topologies is found to exhibit a non-Arrhenius behavior at temperatures above T_m indicating an entropy-driven process, while the renaturation of the 26CEB parallel topology is found to be enthalpy-driven with an activation barrier of a few kcal/mol. This difference could be attributed to the constrained folding landscape of the parallel

topology stemming from the two short propeller loops, the long central loop likely playing a limited role on the coiled DNA strand entropy. Future studies by using this new experimental approach of G4 folding processes will be carried on several CEB25 variants in order to disentangle the effect of the central loop length on the thermal denaturation and renaturation dynamics of this parallel topology.

ASSOCIATED CONTENT

Supporting Information. The support information is available free of charge at UV and CD melting curves; determination of the melting temperatures; *in situ* measurement of the temperature on the T-jump set-up; data analysis; additional T-jump measurements (PDF)

AUTHOR INFORMATION

Corresponding Author

Pascale Changenet − Laboratoire d'Optique et Biosciences, Ecole Polytechnique, CNRS - INSERM, Institut polytechnique de Paris, 91128 Palaiseau Cedex, France; orcid.org/0000-0002-5874-6249; Email: pascale.changenet-barret@polytechnique.edu

Author Contributions

KL and MS carried out the TRCD experiments, FW measured the SRCD of the samples, PC and FH directed the project and wrote the manuscript.

ACKNOWLEDGMENT

This research was supported by Labex PALM (project QUADFold). M. Schmid acknowledges the financial support from RTRA Triangle de la Physique (CD-quadruplex). SRCD measurements on the DISCO beamline at the SOLEIL Synchrotron were performed under proposals 20170318 and 20201655. Authors thanks Jean-Marc Sintès and Xavier Solinas for

technical support on the T-jump set-up and Jean-Louis Mergny for valuable comments on the manuscript.

REFERENCES

1. Jansson, L. I.; Hentschel, J.; Parks, J. W.; Chang, T. R.; Lu, C.; Baral, R.; Bagshaw, C. R.; Stone, M. D., Telomere DNA G-Quadruplex Folding within Actively Extending Human Telomerase. *Proc. Natl. Acad. Sci. USA* **2019,** *116*, 9350-9359.

2. Spiegel, J.; Adhikari, S.; Balasubramanian, S., The Structure and Function of DNA G-Quadruplexes. *Trends Chem.* **2019,** *2*, 123-136.

3. Tian, T.; Chen, Y.; Wang, S. R.; Zhou, X., G-Quadruplex: A Regulator of Gene Expression and Its Chemical Targeting. *Chem* **2018,** *4*, 1314-1344.

4. Gray, R. D.; Petraccone, L.; Trent, J. O.; Chaires, J. B., Characterization of a K^+-Induced Conformational Switch in a Human Telomeric DNA Oligonucleotide Using 2-Aminopurine Fluorescence. *Biochemistry* **2010,** *49* (1), 179-194.

5. Lane, A. N.; Chaires, J. B.; Gray, R. D.; Trent, J. O., Stability and Kinetics of G-Quadruplex Structures. *Nucleic Acids Res.* **2008,** *36*, 5482-5515.

6. Stadlbauer, P.; Mazzanti, L.; Cragnolini, T.; Wales, D. J.; Derreumaux, P.; Pasquali, S.; Šponer, J., Coarse-Grained Simulations Complemented by Atomistic Molecular Dynamics Provide New Insights into Folding and Unfolding of Human Telomeric G-Quadruplexes. *J. Chem. Theory Comput.* **2016,** *12*, 6077-6097.

7. Li, W.; Hou, X. M.; Wang, P. Y.; Xi, X. G.; Li, M., Direct Measurement of Sequential Folding Pathway and Energy Landscape of Human Telomeric G-quadruplex Structures. *J. Am. Chem. Soc.* **2013,** *135*, 6423-6426.

8. Long, X.; Parks, J. W.; Bagshaw, C. R.; Stone, M. D., Mechanical Unfolding of Human Telomere G-Quadruplex DNA Probed by Integrated Fluorescence and Magnetic Tweezers Spectroscopy. *Nucleic Acids Res*. **2013,** *41*, 2746-2755.

9. Okamoto, K.; Sannohe, T.; Mashimo, T. S., H; Terzima, M., G-Quadruplex Structures of Human Telomere DNA Examined by Single Molecule FRET and BrG-Substitution. *Biorg. Med. Chem*. **2008,** *16*, 6873-6879.

10. Gray, R. D.; Trent, J. O.; Chaires, J. B., Folding and Unfolding Pathways of the Human Telomeric G-Quadruplex. *J. Mol. Biol*. **2014,** *426*, 1629-1650.

11. You, J.; Li, H.; Lu, X. M.; Li, W.; Wang, P. Y.; Dou, S. X.; Xi, X. G., Effects of Monovalent Cations on Folding Kinetics of G-Quadruplexes. *Biosci. Rep*. **2017,** *37*, BSR201770771.

12. Zhang, A. Y. Q.; Balasubramanian, S., The Kinetics and Folding Pathways of Intramolecular G-Quadruplex Nucleic Acids. *J. Am. Chem. Soc*. **2012,** *134*, 19297-19308.

13. del Villar-Guerra, R.; Trent, J. O.; Chaires, J. B., G-Quadruplex Secondary Structure Obtained from Circular Dichroism Spectroscopy. *Angew. Chem. Int. Ed*. **2018,** *57*, 7171-7175.

14. Craig, M. E.; Crothers, D. M.; Doty, P., Relaxation Kinetics of Dimer Formation by Self Complementary Oligonucleotides. *J. Mol. Biol*. **1971,** *62* (2), 383-401.

15. Wetmur, J. G., Hybridization and Renaturation Kinetics of Nucleic-Acids. *Annu. Rev. Biophys. Bioeng*. **1976,** *5*, 337-361.

16. Ma, H.; Wan, C.; Wu, A.; Zewail, A. H., DNA Folding and Melting Observed in Real Time Redefine the Energy Landscape. *Proc. Natl. Acad. Sci*. **2007,** *104* (3), 712-716.

17. Narayanan, R.; Zhu, L.; Velmurugu, Y.; Roca, J.; Kuznetsov, S. V.; Prehna, G.; Lapidus, L. J.; Ansari, A., Exploring the Energy Landscape of Nucleic Acid Hairpins Using Laser Temperature-Jump and Microfluidic Mixing. *J. Am. Chem. Soc.* **2012,** *134* (46), 18952-18963.

18. Sanstead, P. J.; Stevenson, P.; Tokmakoff, A., Sequence-Dependent Mechanism of DNA Oligonucleotide Dehybridization Resolved through Infrared Spectroscopy. *J. Am. Chem. Soc.* **2016,** *138* (36), 11792-11801.

19. Menssen, R. J.; Tokmakoff, A., Length-Dependent Melting Kinetics of Short DNA Oligonucleotides Using Temperature-Jump IR Spectroscopy. *J. Phys. Chem. B* **2019,** *123* (4), 756-767.

20. Sanstead, P. J.; Tokmakoff, A., Direct Observation of Activated Kinetics and Downhill Dynamics in DNA Dehybridization. *J. Phys. Chem. B* **2018,** *122* (12), 3088-3100.

21. Gray, R. D.; Trent, J. O.; Sengodagounder, A.; Chaires, J. B., Folding Landscape of a Parallel G-Quadruplex. *J. Phys. Chem. Lett.* **2019,** *10*, 1146-1151.

22. Ashwood, B.; Lewis, N. H. C.; Sanstead, P. J.; Tokmakoff, A., Temperature-Jump 2D IR Spectroscopy with Intensity-Modulated CW Optical Heating. *J. Phys. Chem. B* **2020,** *124* (39), 8665-8677.

23. Changenet, P.; Hache, F., T-Jump and Circular Dichroism: Folding Dynamics in Proteins and DNA. *Mol. Cryst. Liq. Cryst.* **2019,** *693*, 49-56.

24. Holmstrom, E. D.; Dupuis, N. F.; Nesbitt, D. J., Pulsed IR Heating Studies of Single-Molecule DNA Duplex Dissociation Kinetics and Thermodynamics. *Biophys. J.* **2014,** *106*, 220–231.

25. Polinkovsky, M. E.; Gambin, Y.; Banerjee, P. R.; Erickstad, M. J.; Groisman, A.; Deniz, A. A., Ultrafast Cooling Reveals Microsecond-Scale Biomolecular Dynamics. *Nat. Commun.* **2014,** *5*, 5737.

26. El-Harakany, A. A.; Abdel Halim, F. M.; Barakat, A. O., Dissociation Constants and Related Thermodynamic Quantities of the Protonated Acid Form of Tris-(hydroxymethyl)-aminomethane in Mixtures of 2-Methoxyethanol and Water at Different Temperatures. *Electroanal. Chem.* **1984,** *162*, 285-305.

27. Khuc, M. T.; Mendonça, L.; Sharma, S.; Solinas, X.; Volk, M.; Hache, F., Measurement of Circular Dichroism Dynamics in a Nanosecond Temperature-Jump Experiment. *Rev. Sci. Instrum.* **2011,** *82*, 054302.

28. Kubelka, J., Time-Resolved Methods in Biophysics. 9. Laser Temperature-Jump Methods for Investigating Biomolecular Dynamics. *Photochem. Photobiol. Sci.* **2009,** *8*, 499-512

29. Lim, K. W.; Ng, V. C. M.; Martin-Pintado, N.; Heddi, B.; Phan, A. T., Structure of the Human Telomere in Na^+ Solution: an Antiparallel (2+2) G-Quadruplex Scaffold Reveals Additional Diversity. *Nucleic Acids Res.* **2013,** *41*, 10556-10562.

30. Wang, Y.; Patel, D. J., Solution Structure of the Human Telomeric Repeat $d[AG_3(T_2AG_3)_3]$ G-Tetraplex. *Structure* **1993,** *1* (4), 263-82.

31. Neidle, S., Human Telomeric G-Quadruplex: The Current Status of Telomeric G-Quadruplexes as Therapeutic Targets in Human Cancer. *FEBS J.* **2010,** *277* (5), 1118-1125.

32. Aviñó, A.; Fàbrega, C.; Tintoré, M. a.; Eritja, R., Thrombin Binding Aptamer, More than a Simple Aptamer: Chemically Modified Derivatives and Biomedical Applications. *Curr. Pharm. Des.* **2012,** *18*, 2036-2047.

33. Viglasky, V.; Hianik, T., Potential Uses of G-Quadruplex-Forming Aptamers. *Gen. Physiol. Biophys.* **2013,** *32*, 149-172.

34. Reshetnikov, R. V.; Sponer, J.; Rassokhina, O. I.; Kopylov, A. M.; Tsvetkov, P. O.; Makarov, A. A.; Golovin, A. V., Cation Binding to 15-TBA Quadruplex DNA is a Multiple-Pathway Cation-Dependent Process. *Nucleic Acids Res.* **2011,** *39* (22), 9789-9802.

35. Reshetnikov, R.; Golovin, A.; Spiridonova, V.; Kopylov, A.; Sponer, J., Structural Dynamics of Thrombin-Binding DNA Aptamer d(GGTTGGTGTGGTTGG) Quadruplex DNA Studied by Large-Scale Explicit Solvent Simulations. *J. Chem. Theory Comput.* **2010,** *6* (10), 3003-3014.

36. Bian, Y.; Song, F.; Cao, Z.; Zhao, L.; Yu, J.; Guo, X.; Wang, J., Fast-Folding Pathways of the Thrombin-Binding Aptamer G-Quadruplex Revealed by a Markov State Model. *Biophys. J.* **2018,** *114* (7), 1529-1538.

37. Yang, C.; Kulkarni, M.; Lim, M.; Pak, Y., In Silico Direct Folding of Thrombin-Binding Aptamer G-Quadruplex at All-Atom Level. *Nucleic Acids Res.* **2017,** *45* (22), 12648-12656.

38. Zeng, X.; Zhang, L.; Xiao, X.; Jiang, Y.; Guo, Y.; Yu, X.; Pu, X.; Li, M., Unfolding Mechanism of Thrombin-Binding Aptamer Revealed by Molecular Dynamics Simulation and Markov State Model. *Sci. Rep.* **2016**, 24065

39. Kim, E.; Yang, C.; Pak, Y., Free-Energy Landscape of a Thrombin-Binding DNA Aptamer in Aqueous Environment. *J. Chem. Theory Comput.* **2012,** *8* (11), 4845-4851.

40. Schultze, P.; Macaya, R. F.; Feignon, J., Three-dimensional Solution Structure of the Thrombin-binding DNA Aptamer d(GGTTGGTGTGGTTGG). *J. Mol. Biol.* **1994,** *235*, 1532-1547.

41. Masiero, S.; Trotta, R.; Pieraccini, S.; De Tito, S.; Perone, R.; Randazzo, A.; Spada, G. P., A Non-Empirical Chromophoric Interpretation of CD Spectra of DNA G-Quadruplex Structures. *Org. Biomol. Chem.* **2010,** *8*, 2683-2692.

42. Mergny, J. L.; Phan, A. T.; Lacroix, L., Following G-quartet Formation by UV-spectroscopy. *FEBS Lett.* **1998,** *435* (1), 74-78.

43. Majhi, P. R.; Qi, J.; Tang, C.-F.; Shafer, R. H., Heat Capacity Changes Associated with Guanine Quadruplex Formation: An Isothermal Titration Calorimetry Study. *Biopolymers* **2008,** *89*, 302-309.

44. Tucker, B. A.; Hudson, J. S.; Ding, L.; Lewis, E.; Sheardy, R. D.; Kharlampieva, E.; Graves, D., Stability of the Na^+ Form of the Human Telomeric G-Quadruplex: Role of Adenines in Stabilizing G-Quadruplex Structure. *ACS Omega* **2018,** *3*, 844-855.

45. Viglasky, V.; Tluckova, K.; Bauer, L., The First Derivative of a Function of Circular Dichroism Spectra: Biophysical Study of Human Telomeric G-Quadruplex. *Eur. Biophys. J.* **2011,** *40*, 29-37.

46. Martinez-Fernandez, L.; Changenet, P.; Banyasz, A.; Gustavsson, T.; Markovitsi, D.; Improta, R., Comprehensive Study of Guanine Excited State Relaxation and Photoreactivity in G-quadruplexes. *J. Phys. Chem. Lett.* **2019,** *10*, 6873-6877.

47. Schmid, M., *PhD dissertation : Conformational dynamics of G-quadruplex DNA probed by time-resolved circular dichroism*. Univ. Paris-Saclay, 2017.

48. Perez-Arnaiz, C.; Busto, N.; Leal, J. M.; Garcia, B., New Microsecond Intramolecular Reactions of Human Telomeric DNA in Solution. *RSC Advances* **2016,** *6*, 39204-39208.

49. Šponer, J.; Bussi, G.; Stadbauer, P.; Kührova, P.; Banas, P.; Islam, B.; Haider, S.; Neidle, S.; Otyepka, M., Folding of Guanine Quadruplex Molecules-Funnel-Like Mechanism or Kinetic

Partitioning? An Overview from MD Simulation Studies. *Biochim. Biophys. Acta* **2017,** *1861*, 1246-1263.

50. Amrane, S.; Adrian, M.; Heddi, B.; Serero, A.; Nicolas, A.; Mergny, J. L.; Phan, A. T., Formation of Pearl-Necklace Monomorphic G-Quadruplexes in the Human CEB25 Minisatellite. *J. Am. Chem. Soc.* **2012,** *134*, 5807-5816.

51. Piazza, A.; Adrian, M.; Samazan, F.; Heddi, B.; Hamon, F.; Serero, A.; Lopes, J.; Teulade-Fichou, M. P.; Phan, A. T.; Nicolas, A., Short Loop Length and High Thermal Stability Determine Genomic Instability Induced by G-Quadruplex-Forming Minisatellites. *EMBO J.* **2015,** *34*, 1718-1734.

52. Zuffo, M.; Gandolfini, A.; Heddi, B.; Granzhan, A., Harnessing Intrinsic Fluorescence for Typing of Secondary Structures of DNA. *Nucleic Acids Res.* **2020,** *48*, e61.

53. Girdhar, K.; Scott, G.; Chemla, Y. R.; Gruebele, M., Better Biomolecule Thermodynamics from Kinetics. *J. Chem. Phys.* **2011,** *135*, 015102.

54. Gray, R. D.; Chaires, J. B., Kinetics and Mechanisms of K^+- and Na^+-Induced Folding of Models of Human Telomeric DNA into G-Quadruplex Structures. *Nucleic Acids Res.* **2008,** *36*, 4191-4203.

55. Nguyen, T. Q. N.; Lim, K. W.; Phan, A. T., Folding Kinetics of G-Quadruplexes: Duplex Stem Loops Drive and Accelerate G-Quadruplex Folding. *J. Phys. Chem. B* **2020,** *124*, 5122-5130.

56. Long, X.; Stone, M. D., Kinetic Partitioning Modulates Human Telomere DNA G-Quadruplex Structural Polymorphism. *PLoS One* **2013,** *8* (12), e83420.

57. Ying, L.; Green, J. J.; Li, H.; Klenerman, D.; Balasubramanian, S., Studies on the Structure and Dynamics of the Human Telomeric G-Quadruplex by Single-Molecule Fluorescence Resonance Energy Transfer. *Proc. Natl. Acad. Sci. USA* **2003,** *100* (25), 14629-14634.

58. Shirude, P. S.; Balasubramanian, S., Single Molecule Conformational Analysis of DNA G-Quadruplexes. *Biochimie* **2008,** *90*, 1197-1206.

59. Aznauryan, M.; Sondergaard, S.; Noer, S. L.; Schiott, B.; Birkedal, V., A Direct View of the Complex Multi-pathway Folding of Telomeric G-Quadruplexes. *Nucleic Acids Res*. **2016,** *44*, 11024-11032.

60. Noer, S. L.; Preus, S.; Gudnason, D.; Aznauryan, M.; Mergny, J.-L.; Birkedal, V., Folding Dynamics and Conformational Heterogeneity of Human Telomeric G-Quadruplex Structures in Na^+ Solutions by Single Molecule FRET Microscopy. *Nucleic Acids Res*. **2016,** *44* (1), 464-471.

61. Maleki, P.; Budhathoki, J. B.; Roy, W. A.; Balci, H., A Practical Guide to Studying G-Quadruplex Structures Using Single-Molecule FRET. *Mol. Genet. Genom*. **2017,** *292*, 483-498.

62. Mitra, J.; Makurath, M. A.; Ngo, T. T. M.; Troitskaia, A.; Chemla, Y. R.; Ha, T., Extreme Mechanical Diversity of Human Telomeric DNA Revealed by Fluorescence-Force Spectroscopy. *Proc. Natl. Acad. Sci. USA* **2019,** *116* (17), 8350-8359.

63. Gabelica, V., A Pilgrim's Guide to G-Quadruplex Nucleic Acid Folding. *Biochimie* **2014,** *105*, 1-3.

64. Šponer, J.; Islam, B.; Stadlbauer, P.; Haider, S., Molecular Dynamics Simulations of G-Quadruplexes: The Basic Principles and their Application to Folding and Ligand Binding. In *Quadruplex Nucleic Acids as Targets for Medicinal Chemistry*, Neidle, S., Ed. Elsevier: London, 2020; Vol. 54, pp 197-241.

65. Russell, R.; Zhuang, X.; Babcock, H. P.; Millett, I. S.; Doniach, S.; Chu, S.; Herschlag, D., Exploring the Folding Landscape of a Structured RNA. *Proc. Natl. Acad. Sci. USA* **2002,** *99*, 155-160.

66. Hyeon, C.; Thirumalai, D., Mechanical Unfolding of RNA Hairpins. *Proc. Natl. Acad. Sci. USA* **2005,** *102*, 6789-6794.

67. Thirumalai, D.; Klimov, D. K.; Woodson, S. A., Kinetic Partitioning Mechanism as a Unifying Theme in the Folding of Biomolecules. *Theor. Chem. Acc.* **1997,** *96*, 14-22.

68. Wallace, M. I.; Ying, L.; Balasubramanian, S.; Klenerman, D., Non-Arrhenius Kinetics for the Loop Closure of a DNA Hairpin. *Proc. Natl. Acad. Sci. USA* **2001,** *98*, 5584-5589.

69. Dobson, C. M.; Sali, A.; Karplus, M., Protein Folding: a Perspective from Theory and Experiment. *Angew. Chem. Int. Ed.* **1998,** *37*, 868-893.

70. Chen, C.; Wang, W.; Wang, Z.; Wei, F.; Zhao, X. S., Influence of Secondary Structure on Kinetics and Reaction Mechanism of DNA Hybridization. *Nucleic Acids Res.* **2007,** *35*, 2875-2884.

71. Ouldridge, T. E.; Sulc, P.; Romano, F.; Doye, J. P. K.; Louis, A. A., DNA Hybridization Kinetics: Zippering, Internal Displacement and Sequence Dependence. *Nucleic Acids Res.* **2013,** *41* (19), 8886-8895.

72. You, H.; Wu, J.; Shao, F.; Yan, J., Stability and Kinetics of c-MYC Promoter G-Quadruplexes Studied by Single-Molecule Manipulation. *J. Am. Chem. Soc.* **2015,** *137* (7), 2424-2427.

73. Cheng, Y.; Zhang, Y.; Gong, Z.; Zhang, X.; Li, Y.; Shi, X.; Pei, Y.; You, H., High Mechanichal Stability and Slow Unfolding Rates are Prevalent in Parallel-Stranded DNA G-Quadruplexes. *J. Phys. Chem. Lett.* **2020,** *11*, 7966-7971.

74. Ansari, A.; Kuznetsov, S., Is Hairpin Formation in Single-Stranded Polynucleotide Diffusion-Controlled? *J. Phys. Chem. B* **2005,** *109* (26), 12982-12989.

75. Kuznetsov, S. V.; Ansari, A., A Kinetic Zipper Model with Intrachain Interactions Applied to Nucleic Acid Hairpin Folding Kinetics. *Biophys. J.* **2012,** *102*, 101-111.

Folding Dynamics of DNA G-Quadruplexes Probed by Millisecond Temperature Jump Circular Dichroism

K. Laouer[1], M. Schmid[1], F. Wien[2], P. Changenet[1] and F. Hache[1]*

1- Laboratoire d'Optique et Biosciences, Ecole Polytechnique, CNRS-INSERM, Institut Polytechnique de Paris, 91128 Palaiseau Cedex, France.

2- L'Orme des Merisiers, Synchrotron SOLEIL, 91192 Gif sur Yvette, France

Corresponding author : pascale.changenet-barret@polytechnique.edu

Supplementary information

I. UV and CD melting curves

Figure S1 displays the UV melting curves registered by heating and cooling of the G4s, showing the absence of hysteresis in the denaturation and renaturation processes of DNA.

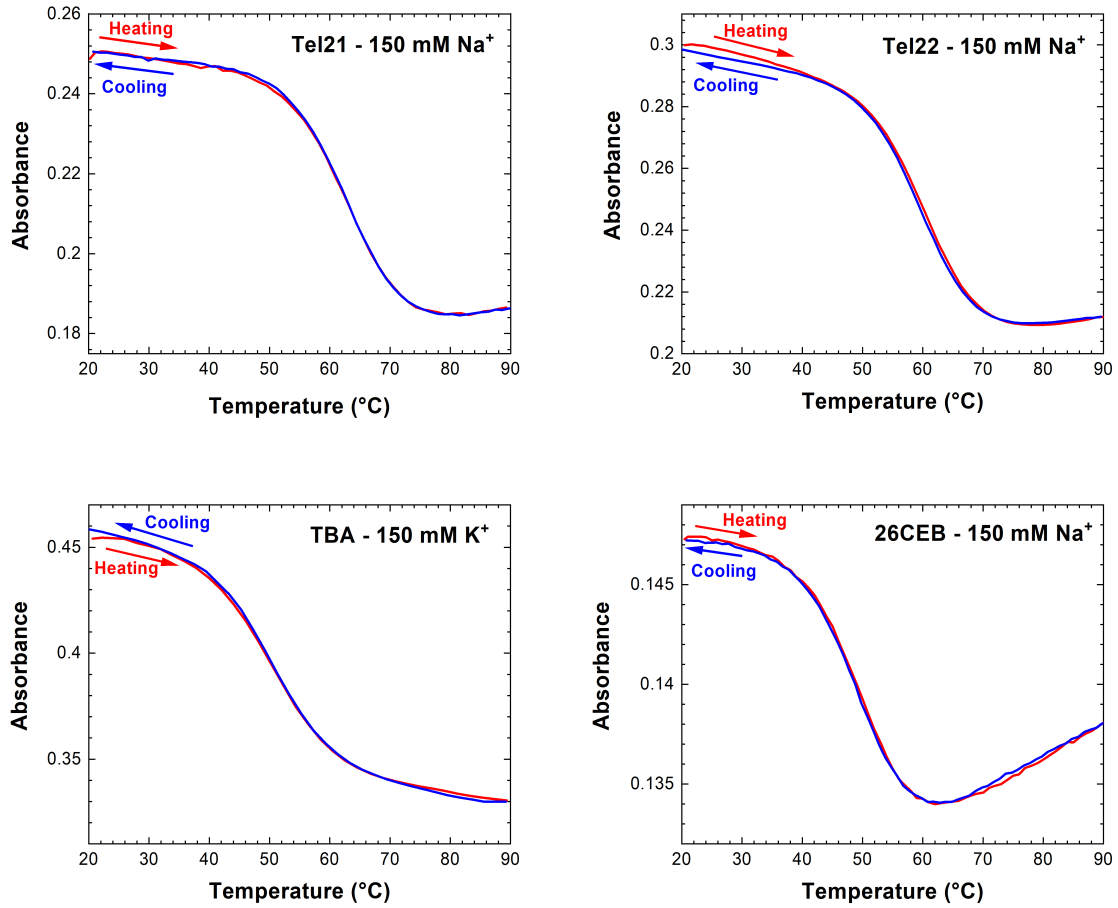

Figure S1: UV melting curves measured at 293 nm for solutions of Tel21, Tel22 and 26CEB with 150 mM Na^+ and a solution of TBA with 150 mM K^+. Red and blue curves correspond to measurements for increasing and decreasing temperatures at a rate of 1°C/min, respectively.

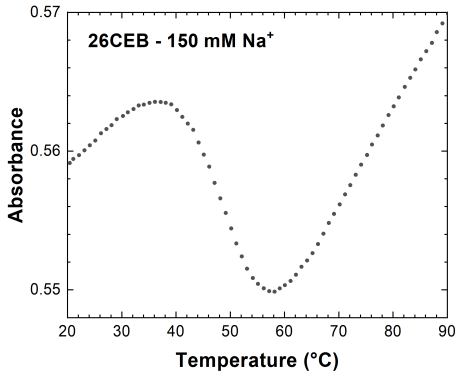

Figure S2: UV melting curve measured at a rate of 1°C/min, at 265 nm, for a solution of 26CEB with 150 mM Na^+.

II. Determination of the melting temperatures

The melting temperature (T_m) has been determined at 293 nm or 265 nm from the UV and CD melting according the procedure described in ref. 1. In this regard, a simple two-state model assuming an equilibrium between one folded and unfolded state of DNA was used. For UV melting, the unfolded fraction of oligonucleotides can be calculated from the experimental data at 293 nm, *OD(T)*, as follow:

$$N_u(T) = L_B^f - OD(T)/L_B^f - L_B^u \quad (1)$$

With L_B^u and L_B^f, the baselines associated to the unfolded and folded oligonucleotides, respectively. The variation of the unfolded fraction of oligonucleotides as a function of temperature can be expressed as follows:

$$N_u(T) = 1/1 + exp\left[\frac{\Delta H^0}{R}\left(\frac{1}{T} - \frac{1}{T_m}\right)\right] \quad (2)$$

with ΔH^0 the enthalpy of the reaction and R, the gas constant. Such analysis is illustrated on Figure S3. Table S1 gathers the melting temperatures obtained from UV and CD melting.

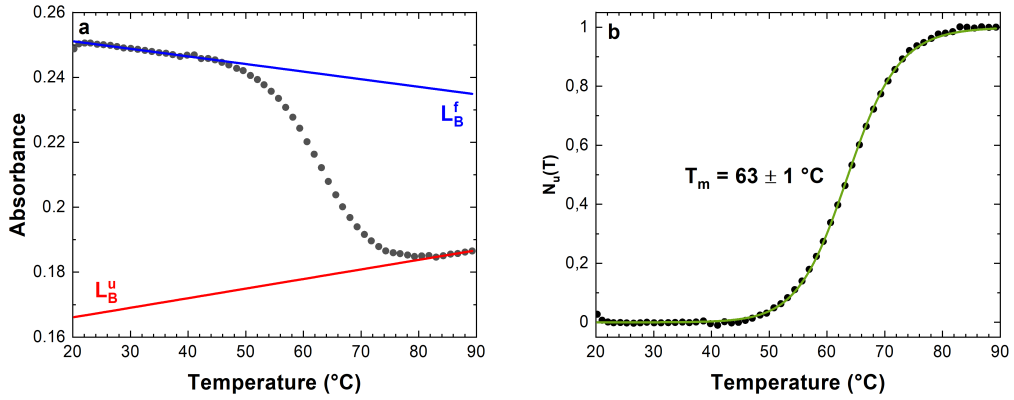

Figure S3: (a) UV melting curve measured at a rate of 1°C/min, at 293 nm, for a solution of Tel21 with 150 mM Na^+. Red and blue lines correspond to the baselines associated to unfolded and folded oligonucleotides, respectively. **(b)** Variation of the unfolded fraction of oligonucleotides, $N_u(T)$, as a function of temperature calculated from the UV melting curve. The green line illustrates the fit of $N_u(T)$ yielding a melting temperature of 63 ± 1 °C.

Sequences	T_m (°C) UV melting	T_m (°C) SRCD melting	T_m (°C) CD melting T-jump
Tel21/150 mM Na^+	63 ± 1 @293 nm	60 ± 2 @293 nm	61 ± 1 @293 nm
Tel21/80 mM Na^+	57 ± 1@293 nm	*not measured*	57 ± 1 @293 nm
Tel22/150 mM Na^+	61 ± 1 @293 nm	58 ± 2 @293 nm	64 ± 1 @293 nm
TBA/150 mM K^+	51 ± 1 @293 nm	49 ± 2 @293 nm	52 ± 1 @293 nm
26CEB/150 mM Na^+	50 ± 1 @293 nm	56 ± 2 @265 nm	54 ± 1 @265 nm

Table S1: Melting temperatures determined from UV melting measurements with a double beam spectrophotometer, SRCD measurements at Soleil synchrotron and CD measurements on the T-jump set-up for Tel21, Tel22, TBA and 26CEB.

III. *In situ* measurement of temperature on the T-jump set-up

The crucial point in T-jump experiments was to determine the temperature change of the sample when it is irradiated by the CW IR diode laser. In this regard, we carried out measurements of the absorbance changes of the phenol red pH indicator in Tris-HCl buffer (100 mM, pH = 7.4) with our double-beam spectrophotometer, as function of the temperature. The pH of the Tris buffer is known to be sensitive to the temperature.[2] In the range between 15°C and 50°C, the phenol red absorbance at 293nm exhibits a linear decrease with a slope of -0.0016 ± 0.0002 /°C. With this value, we could determine the temperature change provoked by the IR irradiation on our T-jump set-up, with a precision of 1°C, which corresponds to a change of 0.0003 in the phenol red absorbance.

We measured the kinetics of the temperature changes for initial temperatures going from 20 to 70 °C and for incident IR power varying between 0.6 to 1.7 W (*i.e.* corresponding to T-jump between 5 and 30°C), at 293 nm. All the kinetics were adjusted with a bi-exponential function with similar time constants. Typically, for increasing temperatures, in the time range between 1 to 5s, we obtained:

$$\Delta T(t) = \Delta T_{max}(1 - Ae^{-\Gamma_1 t} - (1 - A)e^{-\Gamma_2 t}) \quad (3)$$

with $1/\Gamma_1$=14 ms and $1/\Gamma_2$=1300 ms and A=0.83. For decreasing temperatures, in the time range between 5 and 10s, the fits yielded:

$$\Delta T(t) = \Delta T_{max}(Be^{-\Gamma'_1 t} + (1 - B)e^{-\Gamma'_2 t}) \quad (4)$$

with $1/\Gamma'_1$=30 ms and $1/\Gamma'_2$=1700 ms and B=0.82. ΔT_{max} is the maximal temperature change that depends on the incident IR power. Origin of the fast rising and decay component of the sample temperature have been discussed in details in ref. 3 and could be well reproduced by simulations accounting for the equilibration between the heat deposition and the thermal diffusion out of the sample. Note that the thermal conductivity of CaF_2 being more than 16 times greater than that of water, the thermal diffusion out of the sample arises mainly from the sample cell windows and is actually barely sensitive to the solvent.

IV. Data analysis

As shown previously, sample heating and cooling are biphasic processes that should be taken into account in order to extract the intrinsic dynamics of G4s from the experimental data.

1) Intrinsic G4 dynamics: two-state model

We consider first a simple two-state model considering the equilibrium between a folded and an unfolded state:

$$N_f \underset{k_f}{\overset{k_u}{\rightleftharpoons}} N_u$$

with N_f and N_u the population of folded and unfolded G4 DNA strands. Defining α_f and α_u the absorption coefficients of the folded and the unfolded states, the sample absorption reads:

$$\alpha = N_f(t)\alpha_f + N_u(t)\alpha_u \quad (5)$$

When the temperature changes, the fraction of unfolded population changes by $\Delta N_u(t)$, the change of the sample absorption as a function of time is expressed as follow:

$$\Delta\alpha(t) = \Delta N_u(t) \cdot (\alpha_u - \alpha_f) \quad (6)$$

with $\Delta N_u(t) = N_u(t) - N_u(0)$ corresponding to the temporal change of the unfolded fraction of population after the temperature jump. Introducing a unique relaxation rate $\gamma = k_f + k_u$, the dynamical equation governing the evolution of this change reads as:

$$\Delta N_u(t)/dt = -\gamma[\Delta N_u(t) - \Delta N_u(T_{final})] \quad (7)$$

$$\Delta N_u(t) = \Delta N_u(T_{final}) \cdot (1 - e^{-\gamma t}) \quad (8)$$

with $\Delta N_u(T_{final})$, the difference in the fraction of the unfolded population before and after the T-jump, which can be readily obtained from the melting curves.

2) "Deconvolution" of the G4 thermal dynamics

In the above equations, the sample temperature instantaneously reaches its final value, which is not the case in the present T-jump experiments. To account for the biphasic rise of the sample temperature (*T(t)*) to its final value during the denaturation process, the following equation must be solved:

$$d\Delta N_u(t)/dt = -\gamma[\Delta N_u(t) - \Delta N_u(T(t))] \quad (9)$$

In order to fit our experimental data, $\Delta N_u(T(t))$ is replaced by the following biexponential phenomenological function derived from *in situ* measurements of the dynamics change of the sample temperature upon the T-jump (eq. 3). The analytical solution of eq. 9 can be therefore expressed as follow:

$$\Delta N_u(t) = \Delta N_u(T_{final})\left[1 + \frac{p}{\gamma-\Gamma_1}(\Gamma_1 e^{-\gamma t} + \gamma e^{-\Gamma_1 t}) + \frac{1-p}{\gamma-\Gamma_2}(\Gamma_2 e^{-\gamma t} + \gamma e^{-\Gamma_2 t})\right] \quad (10)$$

Although eq. 10 looks quite complicated, it only depends on two fitting parameters, γ and $\Delta N_u(T_{final})$. p is a fixed fitting parameter corresponding to the fraction of unfolded species at the initial temperature, determined from the melting curves measured on the T-jump set-up. A similar treatment can be done for the renaturation process. Fits of the absorption and CD changes, after T-jump, were performed with the two following equations:

$$\Delta A(t) = \Delta a \times \Delta N_u(t) \quad (11)$$

$$\Delta CD(t) = CD(0) + \Delta cd \times \Delta N_u(t) \quad (12)$$

with Δa and Δcd, the amplitudes of the absorption and the CD changes after the T-jump. $CD(0)$ is the value of the CD signal before the T-jump for t<1s.

3) Instantaneous rise and decay in the absorption and the CD signals after T-jump and cooling down

As it is clearly visible in Figure 6, prominent instantaneous rise and decay are observed in the absorption of 26CEB after T-jump and cooling down. Such effects in T-jump measurements are known to arise from non-cooperative events that also appear as the baselines in the UV melting curves of G4s. As shown in Figure S1, these non-cooperative effects are particularly strong for 26CEB at 265 nm but also visible in a lesser extend for the other sequences at 293 nm. To take into account of these very fast changes in the absorption and the CD signals, after T-jump and cooling down, we added an additional term in the fits evolving proportionally to the sample temperature change.

4) Precision of the fitting parameters

For the thermal denaturation, all fits were performed with three parameters corresponding to the denaturation rate of G4, γ, the difference in the fraction of the unfolded population before and after the T-jump: $\Delta N_u(T_{final})$ and the amplitude of the changes of the absorption and CD signals after the T-jump, a and cd. A similar analysis was also carried out for the G4 thermal renaturation. The two amplitude parameters, $\Delta N_u(T_{final})$, Δa or Δcd, are not completely independent and impair the precision of the fits. However, we estimate that the precision of the parameter γ extracted from the fits is within 20%. Furthermore, all fits being made in the same conditions, the relative values of γ can be more precisely compared and discussed (see Figure 7 in the main text).

V. Additional T-jump measurements

1) Antiparallel topologies

Figure S4 compares the absorption and the CD changes averaged over a long acquisition time. The kinetics are found to be identical within our experimental accuracy.

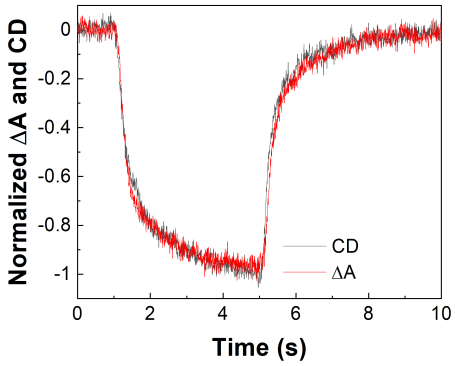

Figure S4: Comparison of the absorption and the CD changes measured for Tel21 with 80 mM Na^+, following a T-jump of 10°C (initial temperature = 40°C) after 1 s and a cooling down after 5 s.

Figure S5 represents the raw experimental curves obtained for Tel21 (a) 80 mM and (b) 150 mM Na^+, together with the expected instantaneous response and the exponential fit (see main text). Lower and higher temperatures have also been measured with visible absorption

changes, but most often the signals were too weak to yield meaningful adjustments. The extracted unfolding times are given in Table I in the main text.

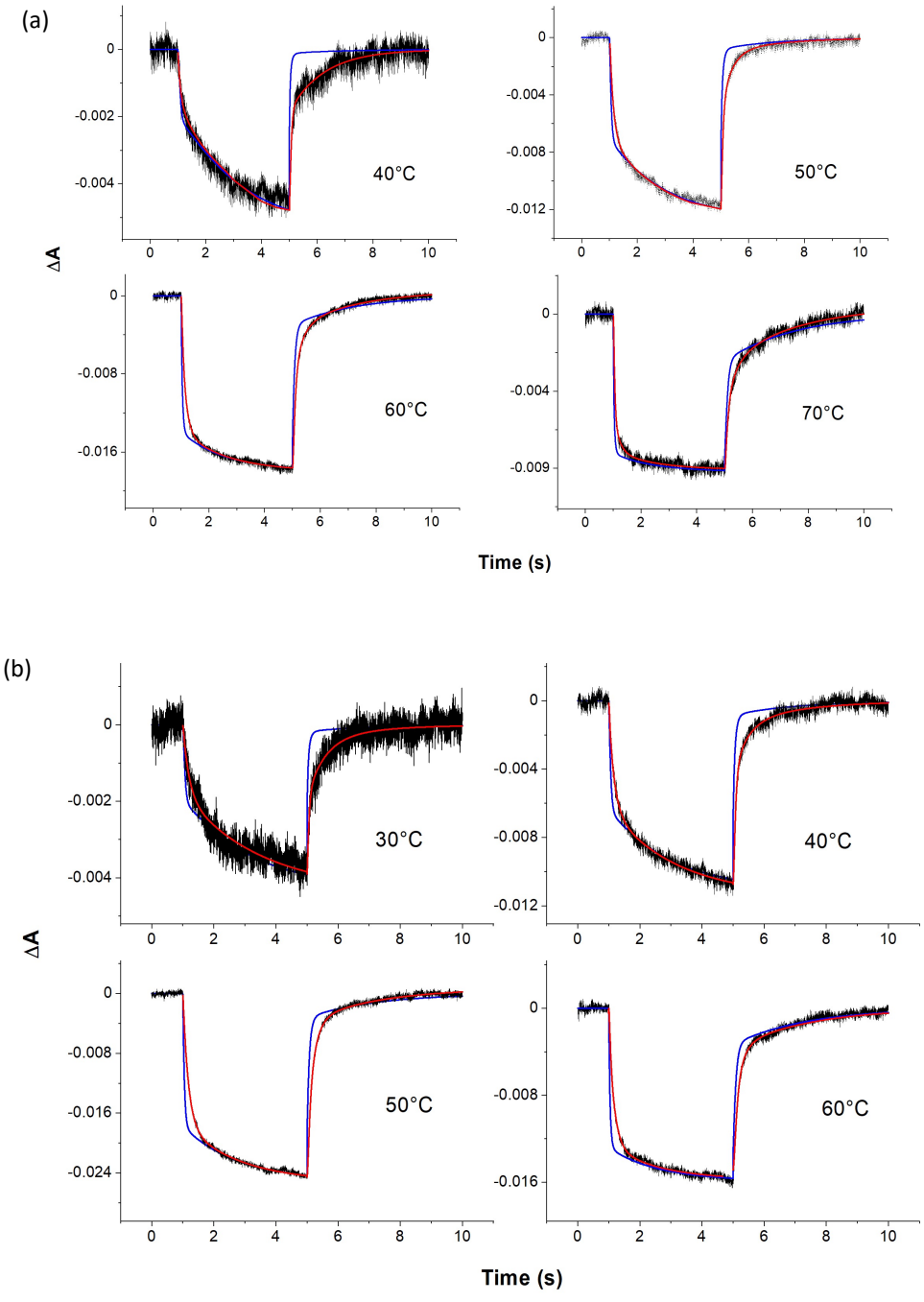

Figure S5: Absorption changes measured for Tel21 with (a) 150 mM and (b) 80 mM Na^+, following a T-jump of 10°C after 1 s and a cooling down after 5 s, for various initial temperatures indicated in each panel. Blue lines correspond to the simulation of the solvent temperature change. Red lines correspond to the fits of the experimental data with a model of two interconverting species "convoluted" with the dynamics of the solvent temperature change.

2) Parallel topology 26CEB

Figure S6 displays typical absorption changes measured at 266 nm for 26CEB with 150 mM Na^+, for an initial temperature of 40°C, after a T-jump and subsequent cooling down of 10°C. The most salient difference with the measurements of the antiparallel topologies performed at at 293 nm is the presence of the prominent instantaneous rise and decay, after T-jump at 1 s and cooling down at 5 s, respectively. These fast changes that follow the temperature rise and decay of the sample are due to non-cooperative events that also appear in the equilibrium UV melting curves as the strong baselines at this specific wavelength in Figure S2. Denaturation and renaturation times extracted from the analytical fits of the absorption changes of 26CEB, for different initial temperatures, are given in Table S2. The fits of the absorption and the CD changes in the time range of a few hundred milliseconds yielded comparable values providing evidence that the same cooperative processes are probed in both cases.

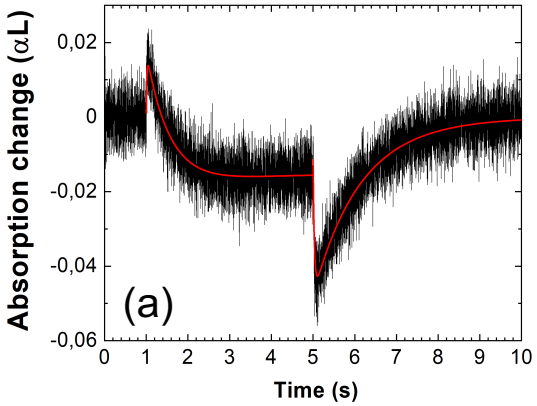

Figure S6: Absorption changes (black lines) at 260nm, measured for 26CEB in the presence of 150 mM Na^+ at 40°C, after a T-jump of 10°C after 1 s and subsequent cooling down to the initial temperature after 5 s. Red lines correspond to the fits of the experimental data with a model of two interconverting species "convoluted" with the dynamics of the solvent temperature change.

T(°C)	τ_{Denat} (ms)		τ_{Renat} (ms)	
	Abs	CD	Abs	CD
20	*n.m.*	715	1586	1041
30	682	554	1260	1085
40	368	357	1039	936
50	186	237	741	844
60	*n.m.*	227	687	811
70	*n.m.*	120	*n.m.*	646

Table S2: Thermal denaturation and renaturation times (τ_{Denat} and τ_{Renat}) extracted from the fits of the absorption and the CD changes at 260 nm, measured for 26CEB (150 mM Na^+), after a T-jump and a cooling down of 10°C, for different initial temperatures (n.m.: not measurable).

VI. References

1. Mergny, J. L.; Lacroix, L., Analysis of Thermal Melting Curves. *Oligonucleotides* **2003,** *13*, 515-537.
2. El-Harakany, A. A.; Abdel Halim, F. M.; Barakat, A. O., Dissociation Constants and Related Thermodynamic Quantities of the Protonated Acid Form of Tris-(hydroxymethyl)-aminomethane in Mixtures of 2-Methoxyethanol and Water at Different Temperatures. *Electroanal. Chem.* **1984,** *162*, 285-305.
3. Ashwood, B.; Lewis, N. H. C.; Sanstead, P. J.; Tokmakoff, A., Temperature-Jump 2D IR Spectroscopy with Intensity-Modulated CW Optcal Heating. *J. Phys. Chem. B* **2020,** *124* (39), 8665-8677.